Journal of the Mechanics and Physics of Solids 61 (2013) 489–503

Contents lists available at SciVerse ScienceDirect

Journal of the Mechanics and Physics of Solids

journal homepage: www.elsevier.com/locate/jmps

Prediction of fracturess toughness of ceramic composites as function of microstructure: II. analytical model

Yan Li [a], Min Zhou [a,b,*]

[a] The George W. Woodruff School of Mechanical Engineering School of Materials Science and Engineering Georgia Institute of Technology, Atlanta, GA 30332-0405, USA

[b] WCU Program on Multiscale Mechanical Design School of Mechanical and Aerospace Engineering Seoul National University, Seoul, Korea

ARTICLE INFO

Article history:
Received 14 February 2012
Received in revised form
12 August 2012
Accepted 11 September 2012
Available online 2 October 2012

Keywords:
Crack deflection/penetration
Fracture toughness
Microstructure–fracture toughness relations
Energy criterion

ABSTRACT

Microstructure and constituent properties combine to determine the overall fracture toughness of particle-reinforced brittle composites through the activation of different fracture mechanisms. The toughening is through increases in energy dissipation when cracks are forced to follow tortuous paths. Based on the results of numerical simulations, a semi-empirical model is developed to predict the fracture toughness of brittle two-phase ceramic composites as a function of statistically defined morphological attributes of microstructure, constituent properties and interfacial bonding characteristics. The quantification of the fracture toughness is achieved by an assessment of the contributions of different fracture mechanisms including matrix fracture, interfacial debonding and particle cracking to the overall energy release rate. In particular, this assessment involves a statistical characterization of the competition between crack deflection and crack penetration at matrix/reinforcement interfaces using a modified version of the energy criterion of He and Hutchinson which accounts for the effects of finite reinforcement size, phase volume fractions, phase shape and phase distribution. The fracture toughness–microstructure relation obtained can be used to identify trends for materials design. Although the numerical quantification is specific to Al_2O_3/TiB_2 ceramic composites, the approach and the model developed apply to brittle particle-reinforced composites in general.

1. Introduction

Microstructure in terms of geometric distribution of phases, constituent properties and interfacial bonding attributes influences the deformation and failure behavior of heterogeneous materials through the activation of different underlying mechanisms. In particular, the fracture behavior and fracture toughness of materials are determined by the mechanisms through which cracks interact with constituents in microstructures. The establishment of microstructure–fracture resistance relations requires the consideration of associated fracture mechanisms. In Li and Zhou (in press), the overall fracture toughness of two-phase Al_2O_3/TiB_2 ceramics is evaluated as a function of microstructural size scale, phase distribution, phase morphology, phase volume fractions, bulk constituent properties and interfacial bonding stiffness using cohesive finite element simulations and a *J*-integral based approach. The required input for the prediction includes

* Corresponding author at: The George W. Woodruff School of Mechanical Engineering School of Materials Science and Engineering Georgia Institute of Technology, Atlanta, GA 30332-0405, USA. Tel.: +1 404 894 3294; fax: +1 404 894 0186.
E-mail address: min.zhou@gatech.edu (M. Zhou).

0022-5096/$ - see front matter © 2012 Elsevier Ltd. All rights reserved.
http://dx.doi.org/10.1016/j.jmps.2012.09.011

Nomenclature

α, β	Dundurs parameters
a_d	crack extension length along an interface
a_p	crack extension length into reinforcement
A	crack area
ε	bi-elastic constant
$\overline{E}$	effective Young's modulus of the composite material
f	volume fraction
H_m, H_{in}, H_p	fractions of matrix cracking, interface debonding and particle cracking
Φ_m, Φ_{in}, Φ_p	surface energy of matrix cracking, interface debonding and particle cracking
J_d, J_p	energy release rates for crack deflection and crack penetration
K_{IC}^i	initiation fracture toughness
K_{IC}	propagation fracture toughness
K	complex stress intensity factor
K_1, K_2	mode I and mode II stress intensity factors
k_I	amplitude factor
ξ	crack length multiplication factor (CLMF)
μ_i	shear modulus (i=0 or 1)
P_{ij}	two-point correlation functions (i=0 or 1; j=0 or 1)
p	crack deflection probability
$\overline{\rho}$	reinforcement roundness
Q	interfacial bonding strength ratio
R	particle radius
S	characteristic reinforcement size
T_{max}^{in}	interfacial bonding strength
T_{max}^{0}	baseline reference bonding strength
U_0	parameter in He and Hutchinson's crack deflection criterion
U	parameter in modified crack deflection criterion
U_f	total fracture energy released
ν_i	Poisson's ratio (i=0 or 1)
$\overline{\nu}$	effective Poisson's ratio of the composite material
ω	crack incident angle
ω_0	critical crack angle for crack deflection
W	total projected crack length

statistical representation of microstructure geometry and characterization of constituent behavior and interfacial bonding. Because statistical measures are used, this approach applies to microstructures with random heterogeneous phase distributions and fracture processes with arbitrary crack paths or micro-crack patterns. In addition to the evaluation of fracture toughness, the CFEM calculations also allowed the trajectories and crack surface areas (crack lengths in 2D) associated with each fracture mechanism (matrix fracture, matrix/reinforcement interfacial debonding and crack penetration of reinforcement particles) during fracture processes to be quantified. Along with the fracture energy of each type of fracture site, the quantification of the crack surface areas makes it possible to calculate the total energy released and, consequently, the overall energy release rate. Here in this paper, the information is used to develop an analytical model for predicting the fracture toughness of such materials as a function of microstructure.

2. Fracture toughness and energy release rate

For brittle materials, the critical energy release rate J_{IC} is rated to the fracture toughness K_{IC} via

$$K_{IC}^2 = J_{IC}\frac{\overline{E}}{1-\overline{\nu}^2}, \tag{1}$$

where $\overline{E}$ and $\overline{\nu}$ are, respectively, the effective Young's modulus and effective Poisson's ratio of the heterogeneous material. For a tortuous crack path involving different types of fracture sites as illustrated in Fig. 1, the average energy release rate

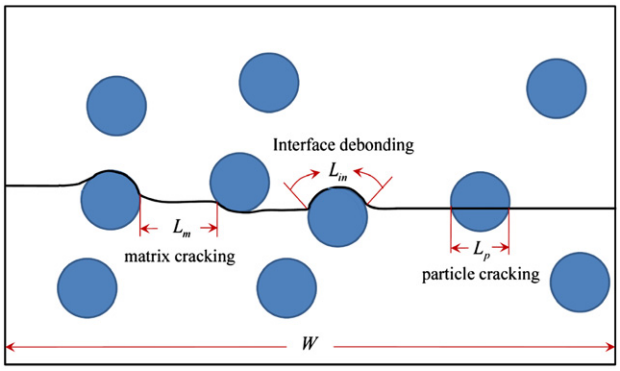

Fig. 1. Schematic illustration of crack trajectory in a two-phase composite and crack lengths associated with different fracture mechanisms.

J can be stated as

$$J_{IC} = \frac{\partial U_f}{\partial A} \approx \frac{(\Phi_{in}L_{in} + \Phi_m L_m + \Phi_p L_p)t_t}{Wt_t}$$
$$= \frac{L}{W}\left(\Phi_{in}\frac{L_{in}}{L} + \Phi_m \frac{L_m}{L} + \Phi_p \frac{L_p}{L}\right)$$
$$= \xi(Q, s, f)(\Phi_{in}H_{in} + \Phi_m H_m + \Phi_p H_p), \tag{2}$$

where U_f is the total energy released to crack surfaces over the projected crack length W, $A=Wt_t$ is the total projected crack surface area with t_t being the specimen thickness. It should be noted that W is the projection of the total curved crack length (arc length L in 2D) in the direction of crack propagation. Specifically, if L_{in}, L_m and L_p represent the crack arc lengths along the interface, within the matrix and through the reinforcement particles, respectively, $L=L_{in}+L_m+L_p$ represents the total crack arc length. Also in Eq. (2), Φ_{in}, Φ_m and Φ_p are the fracture energies for interface debonding, matrix cracking and particle cracking, respectively. $\xi(Q, s, f)=L/W$ can be regarded as the crack length multiplication factor (CLMF). It is a function that captures the influences of interfacial compliance as measured by strength ratio Q, reinforcement size scale s [see Section 4.3 and Eq. (13) in Li and Zhou (in press), respectively], and the volume fraction f of the reinforcement phase. The specific form of this function is unknown. In this paper, the value of ξ is determined empirically by fitting to CFEM data. Details will be given in Section 4. H_{in}, H_m and H_p are the proportions of crack lengths associated with interface debonding, matrix cracking and particle cracking, respectively. Obviously, the evaluation of H_{in}, H_m and H_p is the primary task in order to predict K_{IC} through Eqs. (1) and (2). The specific form is

$$K_{IC} = \sqrt{\frac{\overline{E}}{1-\overline{\nu}^2}J_{IC}} = \sqrt{\frac{\overline{E}}{1-\overline{\nu}^2}\xi(Q, s, f)(\Phi_{in}H_{in} + \Phi_m H_m + \Phi_p H_p)}. \tag{3}$$

It should be pointed out that the analysis embodied in Eqs. (1) through (3) applies only to quasistatic crack growth for which crack speed approaches zero. However, it is important to note that, for brittle materials considered here, the evaluation of J_{IC} (and therefore K_{IC}) can be achieved by properly accounting for the effect of crack speed through fully dynamic calculations, especially when the crack speed is low.

The task of evaluating the right-hand side of Eq. (3) constitutes the bulk of the development below. The interaction between the propagating crack and the reinforcement phase determines L_{in}, L_m and L_p and, consequently, H_{in}, H_m and H_p. There are two possible types of fracture path when a crack approaches a matrix/reinforcement interface in a ceramic composite consisting of a matrix phase and a reinforcement phase. The first fracture mode is interface debonding which is an important fracture mechanism for crack deflection and plays a critical role in material toughening. This mode of fracture is promoted by weak interfacial cohesion, smaller particle size and higher particle roundness. The second fracture mode is particle cracking triggered by crack penetration. This mode of fracture usually signifies catastrophic failure (Hauert et al., 2009; Miserez et al., 2004) and should be avoided as it leads to lower energy release rate because of straight (shorter) fracture paths, even though the fracture energy of the reinforcement phase is higher than those of the interfaces and the matrix phase. Clearly, it is of great importance to quantify the conditions under which the two competing fracture mechanisms are activated. Such a quantification can guide the design and manipulation of microstructures to enhance the fracture resistance of materials through synthesis.

Currently, two approaches exist for determining the activation of the mechanisms. One involves stress-based criteria governed by local asymptotic stress fields at the matrix/particle interfaces (Gupta et al., 1993; Warrier et al., 1997). The other involves energy-based criteria accounting for the differences in the works of fracture along possible alternative crack paths (He and Hutchinson, 1989a, b; Martin et al., 2001). From the energy perspective, a crack would grow when the energy available in the stress field reaches the energy required to form new fracture surfaces along a certain path. The prediction of crack propagation requires the calculation of the energy release rate J as well as a knowledge about the fracture energy Φ. Here, J_d and J_p are used to denote the energy release rate for crack deflection and crack penetration, respectively. Similarly, Φ_{in} and Φ_p denote the fracture energy of the interface and reinforcement, respectively. For brittle materials, crack deflection at an interface requires $J_d \geq \Phi_d$. Crack penetration, on the other hand, requires $J_p \geq \Phi_p$. It is unclear which fracture mechanism would be activated if both conditions are satisfied simultaneously.

He and Hutchinson (1989a, b) analyzed the behavior of a semi-infinite crack perpendicular to an infinite planar interface in a symmetrically loaded, isotropic bi-material, as illustrated in Fig. 2. They argued that crack deflection occurs when

$$J_d/J_p > \Phi_{in}/\Phi_p. \tag{4}$$

Gupta et al. (1992) and (1993) extended He and Hutchinson's work to anisotropic materials and developed a strength criterion for crack deflection and validated their analysis using laser spallation experiments. Subsequently, Martínez and Gupta (1994) improved the criterion such that it does not require any assumption concerning crack extension ratio by using a quasi-static approximation and by assuming that deflection occurs under constant loading. They also showed that the energy criterion for deflection is sensitive to material anisotropy.

Although the above analyses concern the interaction between a single crack and an infinite, flat interface, they reveal some of the fundamental relations that govern the behavior of cracks as they approach interfaces. In this paper, we provide

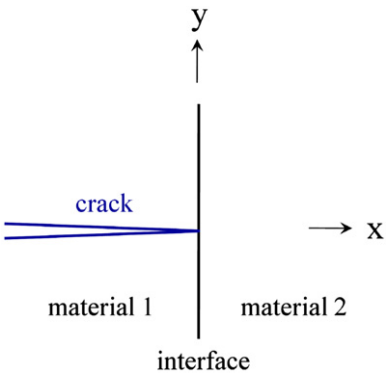

Fig. 2. He and Hutchinson's model of crack deflection/penetration at a bimaterial interface.

an empirical modification of He and Hutchinson's criterion to allow consideration of the effects of finite reinforcement size, reinforcement shape and phase distribution in a two-phase microstructure. Because of the random nature of material heterogeneities at the microstructure level, the interaction of a propagating crack with the phases in a microstructure is rather random. However, over distances longer than the characteristic size scale of the microstructure, the cumulative effect of the random interactions determine the behavior measured at the macroscopic scale. To capture this cumulative effect in the setting of the two-phase ceramic composites consisting of a matrix and a population of reinforcement particles, a measure reflecting the cumulative probability for a crack to encounter the reinforcement phase is used in the modified criterion. This cumulative probability is obtained from the two-point correlation functions. Based on these analyses, a relation between microstructure attributes and overall fracture toughness of the composites is established by assessing the proportion of each fracture mode associated with the crack propagation process. The relation is calibrated using the results of CFEM calculations reported in Li and Zhou (in press).

3. Analytical model for fracture mode selection

Characterization of the competition between crack deflection and crack penetration can allow the proportion of each fracture mode to be quantified. He and Hutchinson (1989a, b) provided an analysis of crack deflection versus penetration at a symmetrically loaded, isotropic bi-material interface. The problem analyzed involves a semi-infinite crack perpendicular to the planar bi-material interface as illustrated in Fig. 2. The solution of this problem depends on Dundurs parameters (Bogy, 1970; Dundurs, 1969) in the forms of

$$\begin{cases} \alpha=[\mu_1(1-\nu_0)-\mu_0(1-\nu_1)]/[\mu_1(1-\nu_0)+\mu_0(1-\nu_1)], \quad and \\ \beta=0.5[\mu_1(1-2\nu_0)-\mu_0(1-2\nu_1)]/[\mu_1(1-\nu_0)+\mu_0(1-\nu_1)]. \end{cases} \tag{5}$$

Here, μ_i and ν_i are the shear modulus and Poisson's ratio respectively for matrix Al_2O_3 ($i=0$) and reinforcement TiB_2 ($i=1$). Both α and β vanish when the matrix and reinforcement materials are identical.

The stress field ahead of the crack-tip is characterized by

$$\sigma_{xx}=k_I(2\pi y)^{-\lambda} \tag{6}$$

where k_I is the amplitude factor proportional to the applied load, λ is a function of α and β satisfying

$$\cos\lambda\pi = \frac{2(\beta-\alpha)}{1+\beta}(1-\lambda)^2+\frac{\alpha+\beta^2}{1-\beta^2}, \tag{7}$$

as discussed by Zak and Williams (1963).

Along the interface ahead of the crack-tip, the tractions are

$$\sigma_{yy}+i\sigma_{xy}=K(2\pi r)^{-0.5}r^{i\varepsilon}, \tag{8}$$

where r is the distance from the crack-tip, $i=\sqrt{-1}$ and

$$\varepsilon=\frac{1}{2\pi}\ln\left(\frac{1-\beta}{1+\beta}\right) \tag{9}$$

is the bi-elastic constant. It should be noted that $K=K_1+iK_2$ in Eq. (8) is the complex stress intensity factor. K_1 and K_2 are the mode I and mode II stress intensity factors, respectively (Rice, 1988).

It can be shown that the energy release rate for crack penetration is

$$J_p=\frac{1-\nu_1}{2\mu_1}K_1^2=\frac{1-\nu_1}{2\mu_1}z^2k_I^2a_p^{1-2\lambda}, \tag{10}$$

where z is a dimensionless function of α and β(He and Hutchinson, 1989a), k_I is amplitude factor, and a_p is the crack extension length into the reinforcement.

Similarly, the energy release rate for crack deflection is

$$J_d = \left(\frac{1-\nu_1}{\mu_1} + \frac{1-\nu_2}{\mu_2}\right)\frac{\left(K_1^2+K_2^2\right)}{4\cosh^2(\pi\varepsilon)}, \tag{11}$$

where

$$K_1^2+K_2^2 = k_I^2 a_d^{1-2\lambda}[|c|^2+|h|^2+2R_e(ch)], \tag{12}$$

with a_d being the crack extension length along the interface. c and h are functions of α and β whose expressions will be discussed later.

He and Hutchinson (1989a) assume that $a_d=a_p$ so that J_d/J_p is independent of the crack extension lengths. The analysis uses the parameter

$$U_0 = \frac{J_d}{J_p} - \frac{\Phi_{in}}{\Phi_p} = \frac{1-\beta^2}{(1-\alpha)z^2}\left[|c|^2+|h|^2+2R_e(ch)\right] - \frac{\Phi_{in}}{\Phi_p} \tag{13}$$

to determine the activation of the fracture mechanisms. Crack deflection is predicted when $U_0>0$, otherwise, crack penetration into the reinforcement phase is expected. In the above relation, J_d,J_p, Φ_{in} and Φ_p are, respectively, the energy release rates of crack deflection and particle penetration and the surface energies of the interface and reinforcement. For the Al_2O_3/TiB_2 ceramic composite system considered in this paper, Φ_{in} and Φ_p are taken as 78.5 J/m^2 and 102.2 J/m^2, respectively. The calculations of the values of z, c and h are discussed in considerable detail by He and Hutchinson (1989a).

To account for the effects of finite particle size, particle shape and microstructure phase distribution, we provide an empirical modification of U_0 in the form of

$$U = \frac{1-\beta^2}{a_0(1-\alpha)}\left[|c|^2+|h|^2+2R_e(ch)\right]\overline{\rho}^{a_1}e^{\left(\frac{a_2}{s}\right)} - \frac{\Phi_{in}}{\Phi_p}, \tag{14}$$

where $\overline{\rho}$ is the roundness of the reinforcement particle, s represents the characteristic reinforcement size which is obtained by fitting the two-point correlation functions as

$$\begin{cases} P_{11} = \left(f-f^2\right)e^{-(D/s)}+f^2, \\ P_{00} = [(1-f)-(1-f)^2]e^{-(D/s)}+(1-f)^2, \ \textit{and} \\ P_{01} = P_{10} = (1-P_{11}-P_{00})/2. \end{cases} \tag{15}$$

Here, P_{ij} denotes the probability for randomly placed vectors of a given length D to start in phase i (i=0 or 1) and ends in phase j (j=0 or 1). In this paper, the matrix is defined as phase 0, while the reinforcement phase is defined as phase 1. For microstructures with randomly distributed circular particles of the same diameter, s is equal to the diameter. The values of s for the microstructures analyzed are given in Fig. 7 of Li and Zhou (in press). P_{01} can be regarded as the geometric probability of encountering the reinforcement phase by a crack of length D that is propagating in the matrix.

To facilitate parametric studies, the coefficient c and h are approximated as (Veljkovic, 2005)

$$\begin{cases} c = \frac{1}{2}\sqrt{\frac{1-\beta}{1+\alpha}}\left(e^{-\frac{i\omega}{2}}+e^{-\frac{3i\omega}{2}}\right), \quad \textit{and} \\ h = \frac{1}{4}\sqrt{\frac{1-\beta}{1-\alpha}}\left(e^{-\frac{i\omega}{2}}-e^{-\frac{3i\omega}{2}}\right), \end{cases} \tag{16}$$

respectively, over the crack incident angle range of $0\le\omega\le\pi/2$ (see Fig. 3).

Implied in Eq. (14) is the fact that smaller and more rounded (Figs. 11 and 16, 17 in Li and Zhou (in press), respectively) particles enhance fracture toughness by inducing crack deflection. It should be noted that U reduces to U_0 for a circular particle ($\overline{\rho}=1$) whose size approaches infinity, since $\lim_{s\to\infty}\overline{\rho}^{a_1}e^{\left(\frac{a_2}{s}\right)}\to 1$. To best describe the CFEM results, the values of the parameters are chosen as a_0=1.3, a_1=0.185 and a_2=5.5 through curve fitting.

As shown in Fig. 3, the crack deflects at the interface when $U>0$, otherwise, it penetrates into the reinforcement and causes particle cracking. The effect of crack incident angle ω is through coefficients c and h in Eq. (16). According to He and Hutchinson (1989a, b), both c and h tend to saturate when $\omega>45^\circ$, as shown in Fig. 4. Furthermore, Veljkovic (2005) has demonstrated that the error associated with the form of c and h in Eq. (16) is within 1% when $0^\circ<\omega<45^\circ$. Therefore, it is quite reasonable to assume that $U(\omega)=U(45^\circ)$ i.e., crack deflects, when $\omega>45^\circ$. The probability of crack deflection is, therefore,

$$p = \frac{\int_{\omega_0}^{\pi/2} U d\omega}{\int_0^{\pi/2}|U|d\omega}. \tag{17}$$

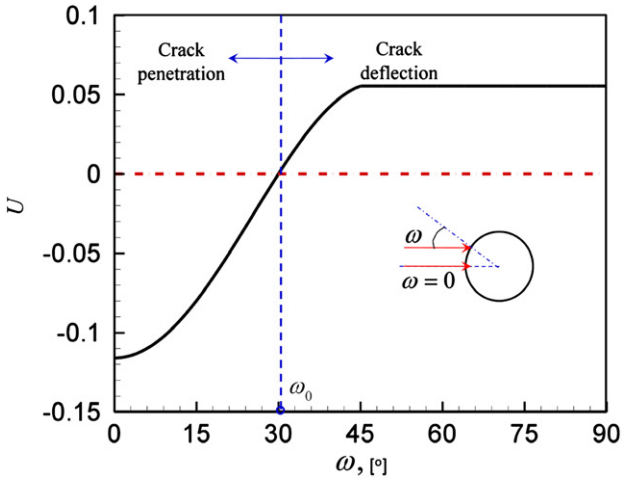

Fig. 3. Parameter U for the determination of crack penetration and crack deflection at a matrix/particle interface.

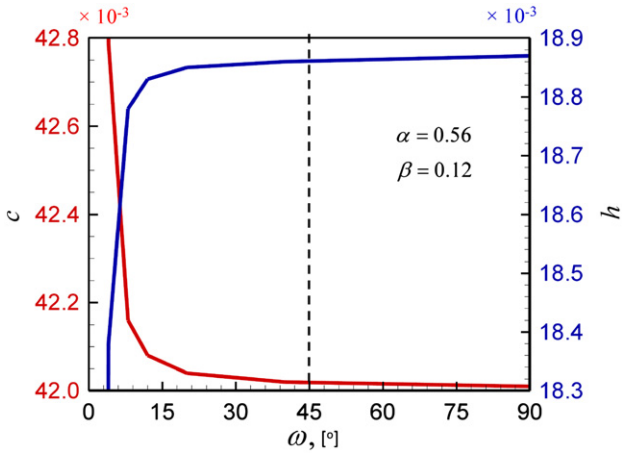

Fig. 4. Dependence of parameter c and h on the crack incident angle ω.

Here, ω_0 denotes the critical crack angle beyond which crack deflection will occur. The likelihood of crack deflection increases as ω increases or as crack direction deviates from the direction normal to the interface, as illustrated in Fig. 3 and shown in Fig. 5. Obviously, $\omega > 0^\circ$ represents the least likely scenario for crack deflection.

Reflecting the trend in the CFEM results, reinforcement size also has a significant impact. As shown in Fig. 5(a) which is generated using Eq. (14), larger particles are more susceptible to crack penetration. The critical size scale for avoiding penetration under the conditions considered is approximately $s=20\,\mu$m for the materials and conditions of the CFEM calculations on which the analysis here is based. This trend is confirmed by the CFEM results shown in Fig. 6. The calculations are carried out under identical conditions, except the size of the particle in front of the crack. As the size of the particle ($\overline{\rho}=1$) increases beyond $s=20\,\mu$m, a fracture mode transition from crack deflection to crack penetration is clearly observed. Under a fixed s, Fig. 5(b, d) shows that higher $\overline{\rho}$ values favor crack deflection and, therefore, enhance K_{IC}. This trend is also confirmed by the CFEM results shown in Fig. 7. Note that the average roundness $\overline{\rho}$ for the circular, square, elliptical and real reinforcements is 1.0, 0.72, 0.62, and 0.62, respectively. As $\overline{\rho}$ decreases from 1 to 0.62, a fracture mode transition from deflection to crack penetration is observed, leading to decreased propagation fracture toughness K_{IC} as illustrated in Figs. 16,17 in Li and Zhou (in press).

4. Microstructure-fracture toughness relation—influences of different mechanisms

To predict K_{IC}, it is important to quantify the probability of occurrence (also referred to as the proportion from here on) for each fracture mechanism over a given crack propagation distance. Here, we take interfacial debonding as an example. The proportion of interfacial debonding over a distance D is the product of (i) the cumulative probability of the crack encountering the reinforcement phase over D and (ii) the probability of crack deflection p. It should be noted that crack deflection can occur through either matrix cracking or interfacial debonding. Therefore, account must be taken of the

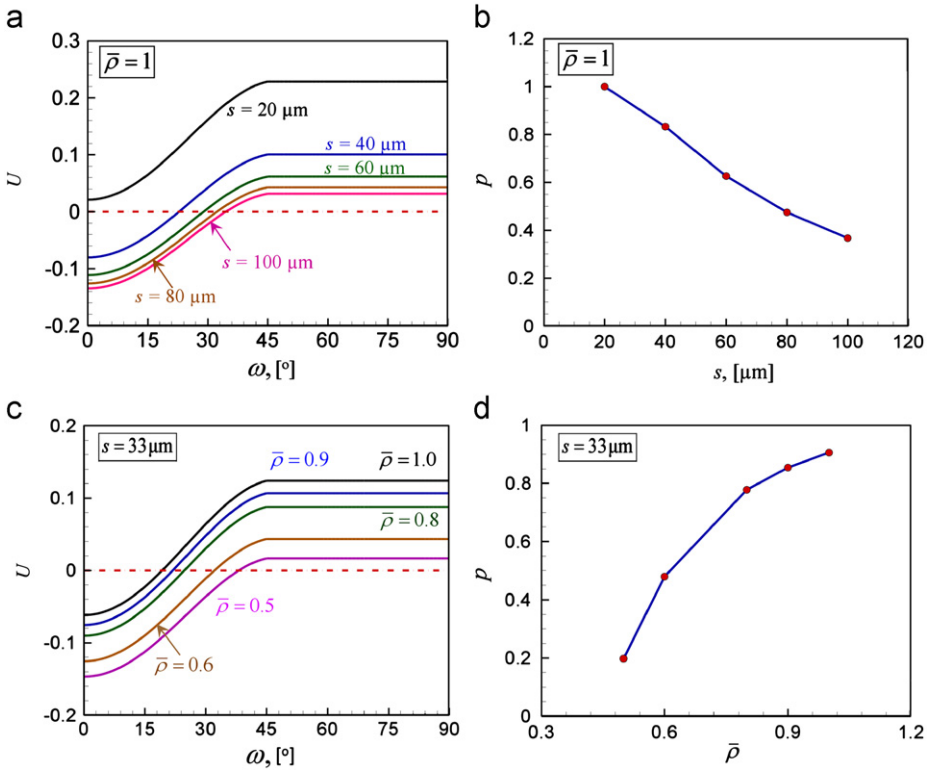

Fig. 5. (a) U as a function of crack incidence angle ω (Fig. 1) for different reinforcement sizes and a fixed mean roundness of 1, (b) effect of reinforcement size on the probability of crack deflection, (c) U as a function of crack incidence angle ω for different reinforcement mean roundness values and a fixed reinforcement size of $s=33$ μm and (d) effect of mean roundness on the probability of crack deflection.

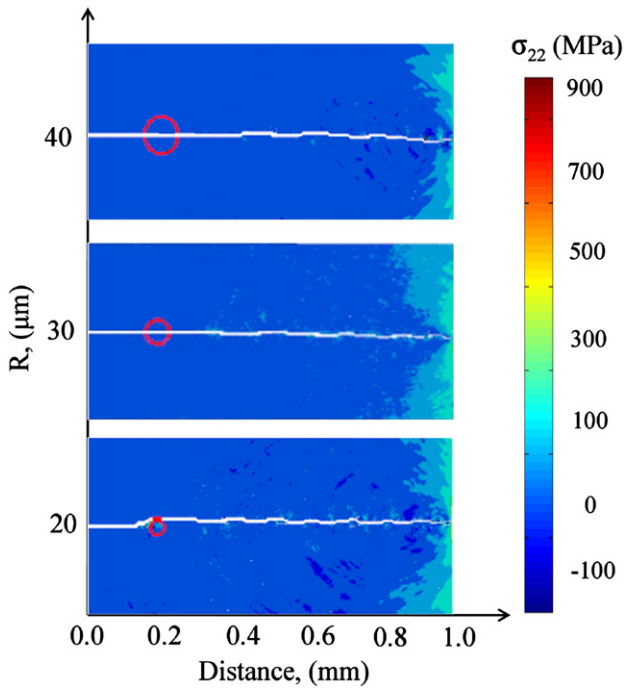

Fig. 6. CFEM results showing the effect of reinforcement size on fracture mode. All conditions except the particle size are the same in the three cases shown.

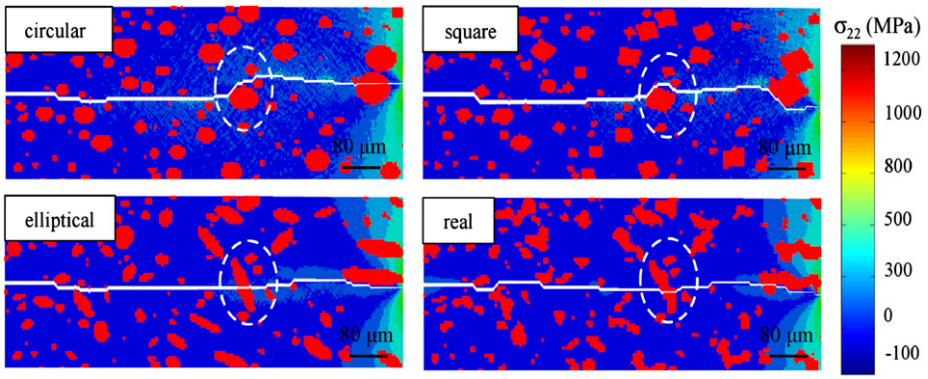

Fig. 7. CFEM results showing the effect of reinforcement roundness on fracture mode. All conditions except the particle shape are the same in the cases shown.

interfacial bonding strength and the fracture energies of the interfaces and the matrix. The relation that accounts for the above factors (fracture mechanism, fracture toughness and microstructure characteristics) can be empirically described as

$$\begin{cases} H_{in}(D) = \dfrac{\int_0^D P_{01}(D)dx}{D} p\left(\dfrac{\Phi_{in}}{\Phi_m}\right)^{-a\ln(Q)}, \\ H_p(D) = \left(\dfrac{\int_0^D P_{01}(D)dx}{D}(1-p) + \dfrac{\int_0^D P_{11}(D)dx}{D}\right)\left(\dfrac{\Phi_{in}}{\Phi_m}\right)^{-b\ln(Q)}, \text{ and} \\ H_m(D) = 1 - H_{in}(D) - H_p(D). \end{cases} \tag{18}$$

Here, H_m,H_{in} and H_p denote the proportions of matrix cracking, interface debonding and particle cracking, respectively. Φ_{in},Φ_m and Φ_p are the fracture energies of the interface, matrix and reinforcement, respectively. Their values are taken as 78.5 J/m^2, 21.5 J/m^2, and 102.2 J/m^2, respectively. a and b are dimensionless parameters determined by fitting the relations to the CFEM results. P_{01} and P_{11} are two-point correlation functions. $Q_1 = T^{in}_{max}/T^0_{max}$ is the interfacial bonding strength ratio, with T^{in}_{max} being the interfacial cohesive strength and T^0_{max} being a baseline reference strength of 0.6 GPa. This reference value is the average value of the cohesive strengths of the matrix and reinforcement. T^{in}_{max} affects the interfacial cohesive energy Φ and has a significant impact on fracture behavior.

In the analysis carried out here, two scenarios are considered. In the first set of calculations, the interfacial cohesive energy Φ is kept constant while T^{in}_{max} and the critical separations (Δ_{tc} and Δ_{nc}) are varied accordingly. The specific range of bounding strength considered here is $10^{-5} \le Q_1 = T^{in}_{max}/T^0_{max} \le 10$. These cases represent very ductile (small Q_1 values) to very brittle interfaces with $Q_1=1$ being the well-bonded case. They can also be regarded as representing very weakly and very strongly bonded interfaces. In the second set of calculations, the critical separation is kept constant at $\Delta_{tc}=\Delta_{nc}=0.068$ μm while T^{in}_{max} and, therefore, the interfacial cohesive energy Φ are varied accordingly. The range of cohesive strength ratio considered in this case is also $10^{-5} \le Q_2 = T^{in}_{max}/T^0_{max} \le 10$. The only difference compared with the first scenario is that the interfaces remain brittle for all the Q_2 cases. It should be noted that the separation needed to achieve full debonding is $\Delta_c=6800$ μm for $Q_1=10^{-5}$, while the interfacial fracture energy is $\Phi=10^{-5}\Phi_{in}$ for $Q_2=10^{-5}$ (Φ_{in} being cohesive energy of the interface for the baseline case of $Q_2=1$). Both situations effectively yield a scenario in which there is essentially no bonding between the two phases. Under these conditions, the calculations represent the behavior of a porous ceramic with the particles being pores. When $Q_1=Q_2=10$, there is negligible differences between the two scenarios since the crack barely goes through the interfaces. The largest discrepancy comes from the range $10^{-3} \le Q_1(Q_2) \le 10^{-1}$. In order to capture the two scenarios, $a=0.4$ and $b=2$ are chosen for the cases with Q_1, while $a=0.63$ and $b=1.54$ are used for cases with Q_2.

To quantify the relative effects, Fig. 8 shows H_{in} and H_p as functions of reinforcement size s and reinforcement volume fraction f. The circular symbols signify the transition in the dominant fracture mechanism under a specific f. On the left side of each transition point (smaller s), interface debonding dominates as H_{in} is always above H_p. On the right hand side (larger s), particle cracking dominates. To maintain the dominance of interface debonding for $10\% \le f \le 25\%$, $s < s_1$ is preferred. When s is within the range of $[s_1, s_2]$, a shift of dominant fracture mode is observed. For example, when $s=65$ μm, particle cracking clearly dominates for $f > 20\%$. This explains the peaking of K_{IC} for $R=30$ μm ($s \approx 2R$) in the CFEM results in Fig. 9. A comparison of the analytical results in Fig. 8 and the CFEM results in Fig. 9 shows that f has little effect on K_{IC} when interfacial debonding is dominant. In contrast, increasing f has a negative effect on K_{IC} when particle cracking is dominant (Miserez et al., 2004).

It is well established that the fracture toughness material can be significantly enhanced through the introduction of compliant interfaces between the matrix and reinforcement (Evans et al., 1991; Roger, 1998). Our CFEM results demonstrate that crack deflection can always be induced if $Q_1(Q_2) < 1$, regardless of the level of interface fracture energy Φ_{in} (Parmigiani and Thouless, 2006). More extensive crack deflection tends to occur at lower $Q_1(Q_2)$ values which leaves the reinforcement intact. The effect of $Q_1(Q_2)$ on fracture mechanisms is systematically captured by Eq. (18). As shown in both plots in Fig. 10, particle cracking can be avoided when $Q_1(Q_2) < 1$. As $Q_1(Q_2)$ decreases, interface debonding gradually

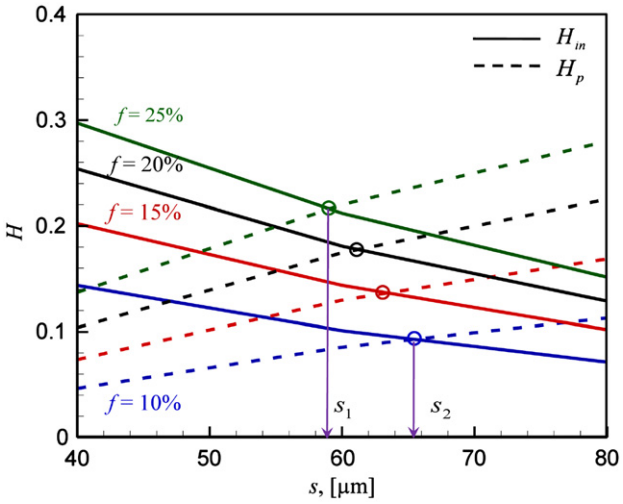

Fig. 8. Proportions of interfacial debonding and particle cracking H_{in} and H_p for different values of s and f.

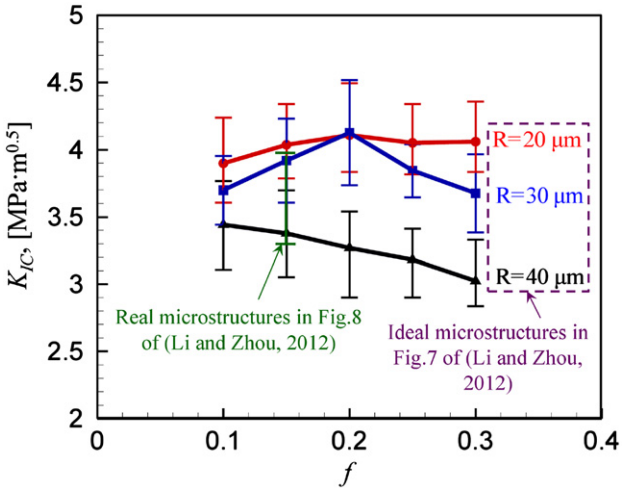

Fig. 9. Effect of reinforcement size and volume fraction on K_{IC}. K_{IC} values are calculated from CFEM simulations at different particle volume fractions and particle sizes.

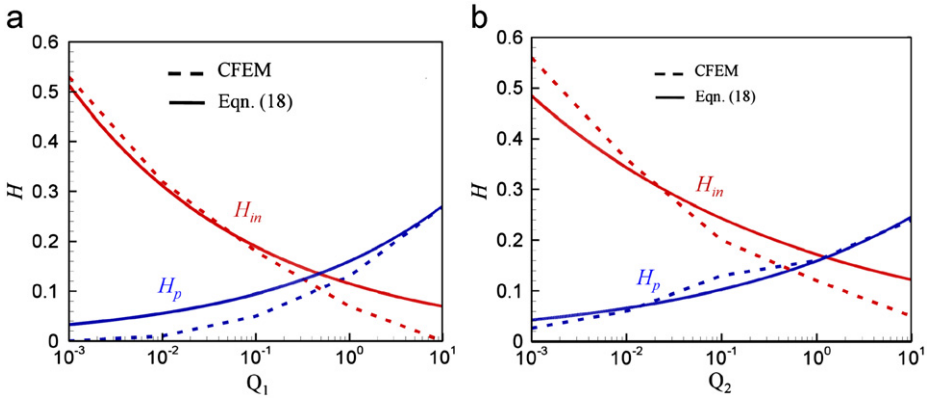

Fig. 10. Comparison of crack proportions H_{in} and H_p as calculated from CFEM simulations and predicted by Eq. (18).

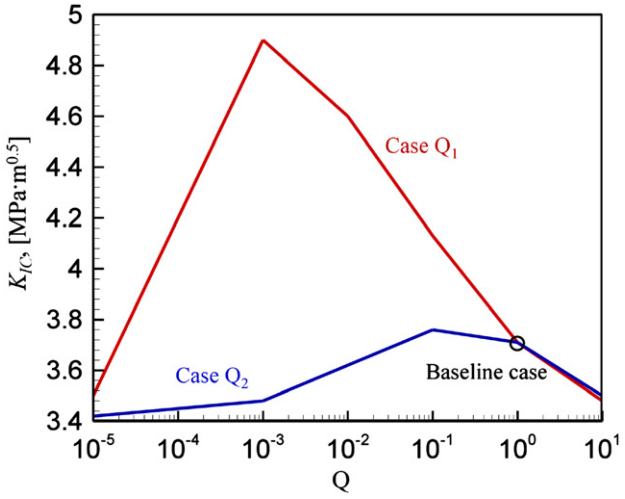

Fig. 11. CFEM results showing the effect of interfacial bonding strength on K_{IC}.

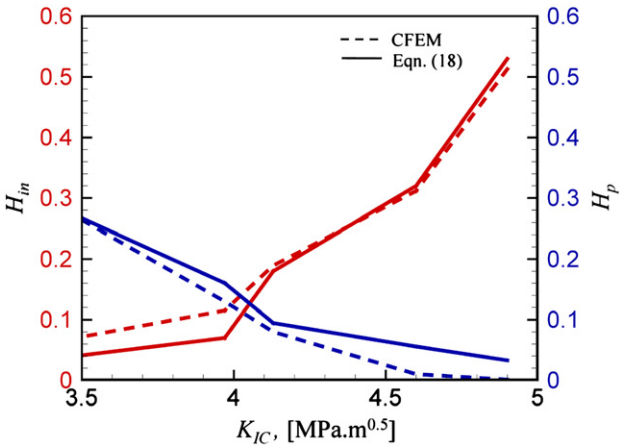

Fig. 12. Effect of interfacial debonding and particle cracking on K_{IC}.

outweighs matrix cracking and becomes the dominant fracture mode. It should be noted that the best toughening results can only be achieved without sacrificing the interfacial fracture energy. As demonstrated in Fig. 11, the improvement in fracture toughness K_{IC} is minor for cases among Q_2 as discussed above, although there is a greater amount of interface debonding compared with the cases with Q_1. This is due to the fact that the interfacial fracture energy drops drastically as Q_2 decreases. Therefore, a proper balance between interfacial compliance and the activation of interface debonding must be maintained to best improve K_{IC}.

The model engendered by Eq. (18) accounts for the effects of both the geometric attributes (characteristic reinforcement size s, volume fraction f, roundness $\overline{\rho}$) and the material attributes (interfacial bonding strength ratio of the interface between the reinforcement and the matrix phase) of the microstructure on the proportion of each fracture mechanism. For the material system analyzed, development of microstructure–fracture toughness relations entails quantitatively correlating the fracture mechanisms with the fracture toughness. To illustrate the point, the K_{IC} values of the microstructures in Figs.7 and 8 of Li and Zhou (in press) are employed. The predicted proportions of interfacial debonding and particle cracking from the CFEM results and the analytical model are compared in Fig. 12. Both the model and the CFEM data show that if the interfacial fracture energy is kept constant as $\Phi_{in}=78.5\ J/m^2$ while the interfacial bonding strength ratio Q_1 varies, the propagation fracture toughness K_{IC} can be improved by 37.2% as the proportion of interfacial debonding increases from approximately 5% to 50%. Moreover, an increase in the fraction of particle cracking by the same magnitude has the opposite effect on K_{IC}.

As discussed previously, the prediction of fracture toughness K_{IC} through Eq. (3) requires the evaluation of $\xi(Q, s, f)$, which is defined as L/W or the crack length multiplication factor (CLMF). Here, L and W are the real arc length and projected crack length, respectively. Since the model we proposed here only considers quasi-static crack propagation, ξ only depends on heterogeneity-induced crack trajectory variation. In this sense, the crack length multiplication factor

$\xi \geq 1$ for all cases. The minimum value of ξ is obtained at $f=0$ and $f=1$ when the whole microstructure is pure matrix or reinforcement, respectively. In both cases, no heterogeneity-induced crack deflection exists and the propagating crack follows the straight trajectory. $\xi(Q, s, f)$ accounts for the influences of interfacial bonding strength, reinforcement size and volume fraction on total crack length. The functional of $\xi(Q, s, f)$ is fitted to the CFEM data using the empirical form

$$\xi(Q, s, f) = \tilde{\xi}(s,f)\tilde{\xi}(Q). \tag{19}$$

Specifically, $\tilde{\xi}(Q)$ is fitted at $s=66.14$ μm and $f=15\%$. To account for both the Q_1 and Q_2 cases, $\tilde{\xi}(Q)$ takes the form

$$\tilde{\xi}(Q) = \begin{cases} n_1 Q_1^{n_2}, \\ n_3 Q_2^{n_4}. \end{cases} \tag{20}$$

Similarly, $\tilde{\xi}(s,f)$ is fitted at $Q=1$, when $\tilde{\xi}(Q=1)$ is taken as a constant. To best represent the CFEM data, $\tilde{\xi}(s,f)$ takes the form of

$$\tilde{\xi}(s,f) = \frac{1-e^{D_2}}{e^{D_1}-e^{D_2}} e^{D_1 f} + \frac{e^{D_1}-1}{e^{D_1}-e^{D_2}} e^{D_2 f} \tag{21}$$

where $D_1 = m_1 s + m_2$ and $D_2 = m_3 s^{m_4} + m_5$.

The parameters $n_1=1.191$, $n_2=-0.044$, $n_3=1.167$, $n_4=-0.047$, $m_1=0.0175$, $m_2=-1.483$, $m_3=-4.7\times10^{-12}$, $m_4=6.695$ are chosen such that the best fit to the data is achieved.

$\xi(Q, s, f)$ can be used to quantitatively explain the counterintuitive phenomenon that microstructures with larger and higher volume fractions of tougher reinforcement particles have lower fracture toughness K_{IC} values (Fig. 9) even though the fracture energy of the particles is 4.75 and 1.3 times of the matrix and interface, respectively. The physical implication of ξ is demonstrated in Fig. 13. The boundary constraints of ξ are well satisfied since $\xi=1$ resides at $f=0$ and $f=1$, as expected. It should be noted that the CFEM data are only available within the solid portion of curves as represented by the error bars. The dashed parts, which are extrapolated according to Eq. (19), also make physical sense. First of all, the increase of reinforcement size tends to decrease ξ across the whole range of volume fraction f. This is in good agreement with the criterion in Eq. (14) as well as the CFEM results in Fig. 9, since small reinforcements promote crack deflection and in turn the tortuosity of the crack path. It can be argued that there exists an upper bound of reinforcement size beyond which ξ approaches 1 (i.e., particle penetration essentially always occurs). As shown in Fig. 14, $s_{max} \approx 85$ μm is predicted as the upper bound of the reinforcement size. As s approaches S_{max}, volume fraction f becomes less important as ξ quickly saturates to 1 due to diminishing crack deflection. Although decreasing s can effectively increase ξ, the lower bound of s cannot be ignored. At $s=0$, the material is essentially the pure matrix with $f=0$. This means decreasing the reinforcement size beyond the lower bound S_{min} adversely influences ξ. Currently, our CFEM model cannot precisely predict the value of s_{min} since the allowed minimum mesh size is 7 μm. However, for most engineering cases, the predicted trend is still valid.

It can be seen from Fig. 13 that the peaks of the curves gradually shift toward the right as s decreases. Specifically, the maximum value of ξ at $s=40$ μm, 60 μm and 80 μm are 1.4263, 1.3083 and 1.0735, for $f=31\%$, 23% and 11%, respectively. The data indicate that particle cracking tends to dominate over interface debonding as f goes beyond each individual thresholds. This again explains the trend in Fig. 9 that at $s=60$ μm, K_{IC} increases with f initially but follows the opposite trend as f goes beyond 20%, which is very close to 23% as predicted above. Besides, the predicted f thresholds at $s=40$ μm and 80 μm also explain the fact that K_{IC} either increases or decreases monotonically with f, since the lower and upper bounds of f considered in our CFEM calculations are 10% and 30%, respectively. The dashed lines in Fig. 14 represent cases

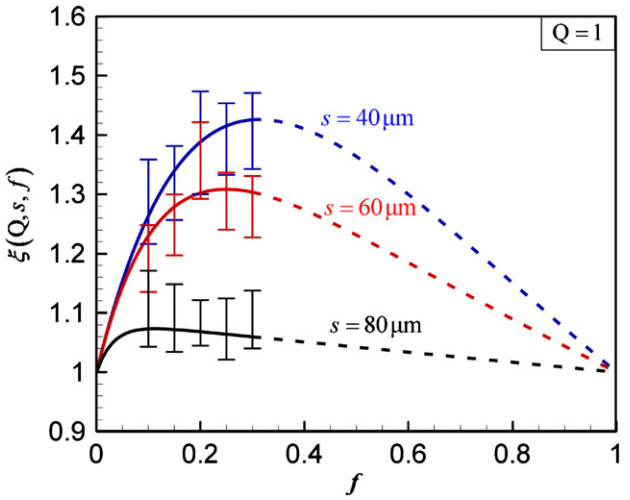

Fig. 13. Effect of reinforcement size s on crack length multiplication factor $\xi(Q, s, f)$.

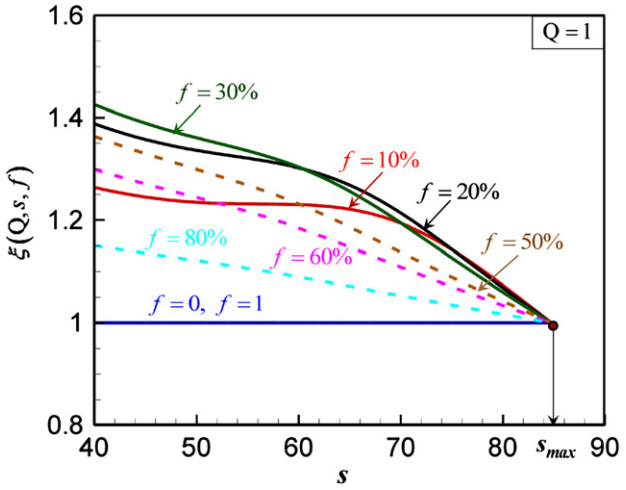

Fig. 14. Effect of reinforcement volume fraction f on crack length multiplication factor $\xi(Q,s,f)$.

that are not considered in the CFEM calculations. It is shown that ξ continuously decreases with f and eventually overlaps with the case at $f=0$ when f increases to 100%. This is consistent with the above discussions and the trend demonstrated in Fig. 13.

In addition to reinforcement size s and volume fraction f, the interfacial bonding strength Q also has a significant influence on ξ. The cases considered in Fig. 15 have the same reinforcement size $s=66.14$ μm and volume fraction $f=15\%$. It is noted from Fig. 15(a) and (b) that ξ follows a very similar trend for both Q_1 and Q_2. ξ tends to reach 1 as crack deflection is gradually eliminated by the increasing interfacial bonding strength. On the other hand, the maximum value of ξ is around 2, suggesting that the largest possible crack length magnification is about two times the projected crack length.

On the other hand, $H_{in}\Phi_{in}+H_m\Phi_m+H_p\Phi_p$ is the equivalent dissipated energy per unit projected crack length. The competition between this term and ξ determines the level of K_{IC}. Fig. 15(c) and (d) show that the value of $H_{in}\Phi_{in}+H_m\Phi_m+H_p\Phi_p$ is lowest when both Q_1 and Q_2 are extremely small, leading to diminishing improvement in K_{IC} even though the corresponding ξ tends to the highest possible value. The diametrically opposite effect but the same outcome is observed for extremely large Q_1 and Q_2 values, when the CLMF ξ is the lowest and moderately high or high $H_{in}\Phi_{in}+H_m\Phi_m+H_p\Phi_p$ values are seen.

Noted that, for both the Q_1 and Q_2 cases, the maximum value of K_{IC} is obtained when ξ and $H_{in}\Phi_{in}+H_p\Phi_p+H_m\Phi_m$ are balanced. Specially, the best improvement of K_{IC} is achieved when the increase in ξ is not at the expense of decreasing $H_{in}\Phi_{in}+H_p\Phi_p+H_m\Phi_m$. To better understand this issue, the individual contributions from different fracture mechanisms to K_{IC} are shown in Fig. 16. For this purpose, note that the contribution to K_{IC}^2 from interface debonding is $\overline{E}\xi(Q,s,f)\Phi_{in}H_{in}/\left(1-\overline{\nu}^2\right)$, from particle cracking is $\overline{E}\xi(Q,s,f)\Phi_pH_p/\left(1-\overline{\nu}^2\right)$,and from matrix cracking is $\overline{E}\xi(Q,s,f)\Phi_mH_m/\left(1-\overline{\nu}^2\right)$. Clearly in Fig. 16(a), K_{IC} is dominated by the effects of interface debonding when the matrix/reinforcement interface is compliant or relatively weak, i.e., $Q_1\in[10^{-5},0.5]$. In contrast, interface debonding makes the least contribution to K_{IC} when $Q_2\in[10^{-5},0.5]$, as illustrated in Fig. 16(b). This is due to the rapid decay of Φ_{in} when $Q_2<1$. On the other hand, the contribution from particle cracking is the largest in both sets of data when Q_1 or $Q_2=10$.

Most importantly, Fig. 16(a) shows that the maximum contribution from particle cracking (which occurs at $Q_1=10$) is less than half of the maximum contribution from interface debonding (which occurs near $Q_1\approx10^{-3}$) even though $\Phi_p=1.3\,\Phi_{in}$ (baseline case). The fundamental reason is that it is more energetically favorable for cracks to propagate along the path that requires the lowest fracture energy. Crack deflection into the matrix/reinforcement interface causes the crack trajectory to become more tortuous, leading to higher ξ. This significantly increases the crack surface area and compensates for the relatively lower fracture energy of the interface. Indeed, as shown in Fig. 10(a), the value of H_{in} can be 16 times the value of H_p (note that the maximum value of the ratio between the two quantities occurs at the left end of the curves), making interface debonding by far the dominant mechanism for altering energy dissipation. Since Φ_{in} does not change with Q_1 for this case, the best strategy to improve K_{IC} is to maximize H_{in} by promoting crack deflection through the optimization of Q_1 rather than to increase the fracture energy of reinforcement Φ_p or the particle volume fraction f. The latter two measures can help, but their effects are very limited as shown in Fig. 17 and Fig. 14. When the cases with varying Q_2 values are considered, maximizing H_{in} through the optimization of Q_2 can still improve K_{IC}. However, the effect becomes less pronounced as the contribution of $H_{in}$to the increase of ξ is much less significant in light of the decrease in Φ_{in}.

In conclusion, the analytical results discussed in this paper and the CFEM results of Li and Zhou (in press) show that the most effective way to improve the fracture toughness of two-phase ceramics composites is to create compliant (ductile)

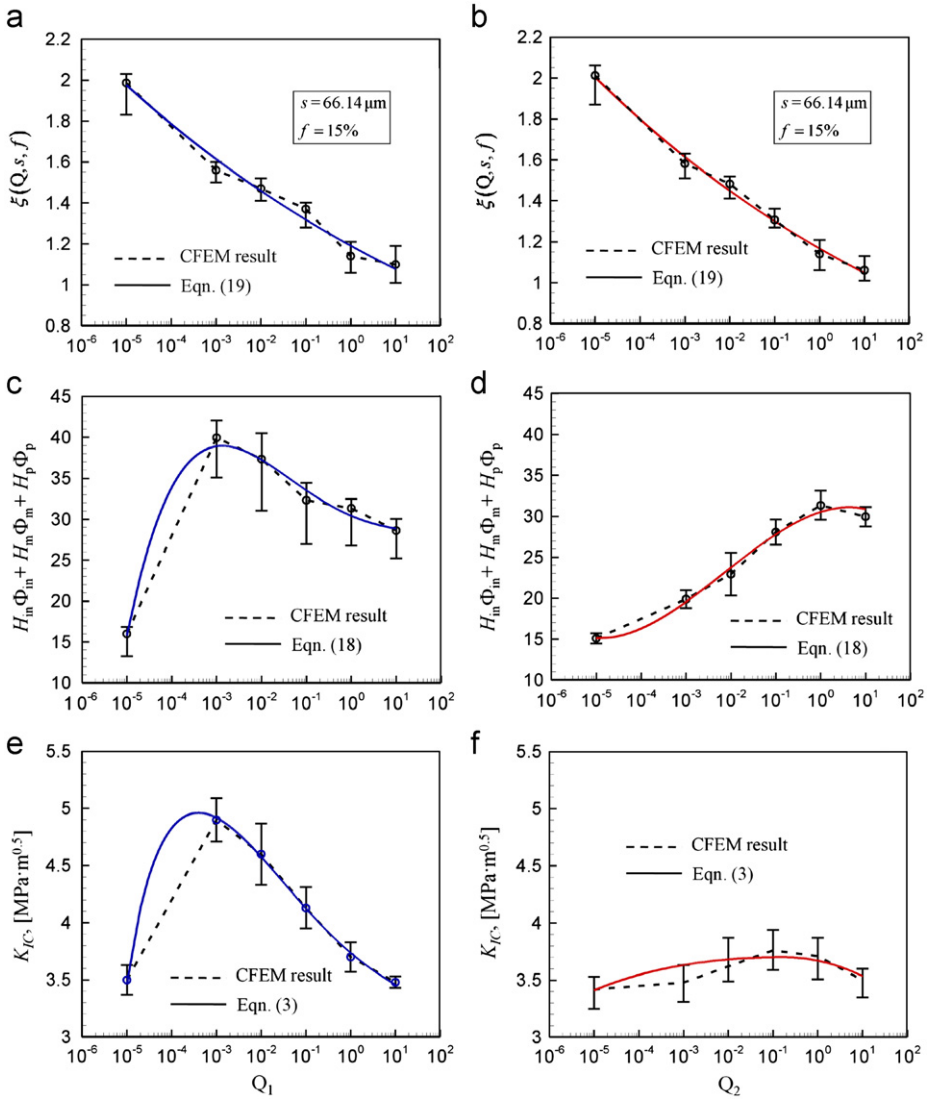

Fig. 15. Effect of interfacial bonding strength ratios, (a). Q_1 on ξ at constant interface fracture energy, (b). Q_2 on ξ at constant critical cohesive separation distance, (c). fracture energy releases per unit crack length for case (a), (d). fracture energy released per unit crack length for case (b), (e). corresponding K_{IC} values for case (a), and (f). corresponding K_{IC} values for case (b).

interfaces with high interfacial fracture energy levels. For the conditions and material system analyzed, the maximum value of K_{IC} occurs at approximately $Q_1 = 10^{-3}$. This result also suggests that currently available ceramic materials (Q_1 or $Q_2 \approx 1$) are not optimized in terms of K_{IC} and room for improvement through means identified here exist. In addition to appropriately configured bonding between the constituents, fracture toughness can also be enhanced through microstructure size scale refinement and the use of reinforcement particles with more rounded morphologies. The model developed can be used to guide the microstructure design of ceramic composites.

5. Summary

An energy-based semi-empirical model is developed to quantify the results of CFEM predictions of fracture toughness of two-phase ceramic composites and to provide an analytical relation between the fracture toughness and microstructure. This semi-empirical model is based on the analytical model of Hu and Hutchinson for the behavior of a crack approaching a planar bi-material interface and accounts for the effects of statistical attributes of microstructures (two-point correlation function, particle size, particle volume fraction, particle shape and phase distribution) and material properties (constituent properties and interfacial bonding strength) by quantifying the probability for the activation of different fracture mechanisms (crack deflection and crack penetration of reinforcement).

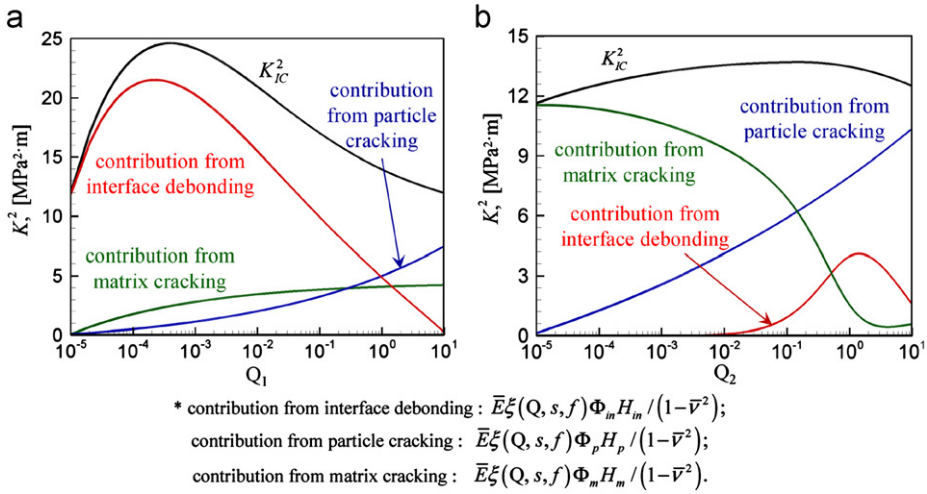

Fig. 16. Contributions of individual fracture mechanism to the overall fracture toughness.

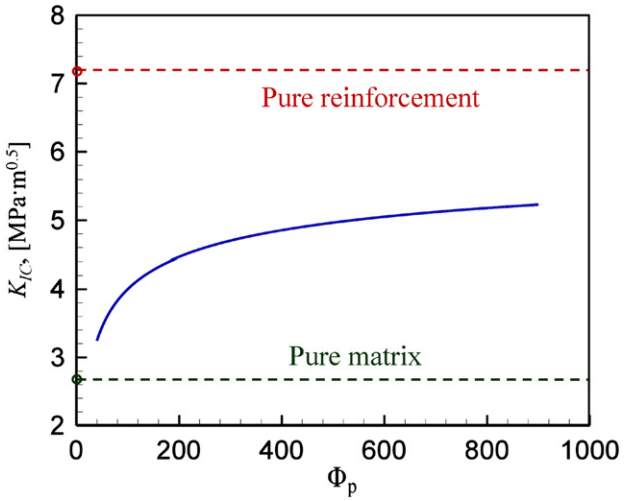

Fig. 17. Effect of reinforcement toughness on K_{IC}.

For ceramic composites systems like the Al_2O_3/TiB_2 composites analyzed here, the competition between crack deflection and reinforcement penetration plays the most important role in determining the dominant fracture mode and in turn the fracture toughness. Results of CFEM calculations and predictions of the semi-empirical model show that both microstructure and constituent properties can significantly influence the fracture behavior and combine to determine the overall fracture toughness through the activation of different fracture mechanisms. The analytical model provides deeper insights into the fracture process as it quantitatively predicts the proportion of each fracture mechanism in the heterogeneous microstructure. To enhance the propagation fracture toughness, fine microstructure size scale, rounded reinforcement morphology and appropriately weak bonding strength should be introduced to promote interface debonding and discourage particle cracking. There is an optimal level of interfacial stiffness that maximizes the fracture toughness. These conclusions can be used in the selection of materials and the design of new materials with tailored properties.

Acknowledgment

This research is primarily supported by the NSF Center for Computational Materials Design (CCMD) at Georgia Institute of Technology and Pennsylvania State University. MZ also acknowledges support from the National Research Foundation of Korea through WCU Grant no. R31-2009-000–10083-0.

References

Bogy, D.B., 1970. Elastostatic solutions on bonded half planes of dissimilar materials. J. Appl. Mech. 37, 220.
Dundurs, J., 1969. Edge-Bonded Dissimilar Orthogonal Elastic Wedges Under Normal and Shear Loading. J. Appl. Mech 36, 650–652.
Evans, A.G., Zok, F.W, Davis, J., 1991. The role of interfaces in fiber-reinforced brittle matrix composites. Compos. Sci. Technol 42, 3–24.
Gupta, V., Argon, A.S., Suo, Z., 1992. Crack Deflection at an Interface Between Two Orthotopic Media. J. Appl. Mech. 59, S79–S87.
Gupta, V., Yuan, J., Martinez, D., 1993. Calculation, Measurement, and Control of Interface Strength in Composites. J. Am. Ceram. Soc. 76, 305–315.
Hauert, A., Rossoll, A., Mortensen, A., 2009. Particle fracture in high-volume-fraction ceramic-reinforced metals: governing parameters and implications for composite failure. J. Mech. Physics. Solids 57, 1781–1800.
He, M.-Y., Hutchinson, J.W., 1989a. Crack deflection at an interface between dissimilar elastic materials. Int. J. Solids. Struct. 25, 1053–1067.
He, M.-Y., Hutchinson, J.W., 1989b. Kinking of a Crack Out of an Interface. J. Appl. Mech. 56, 270–278.
Li, Y., Zhou, M. Prediction of fracture toughness of ceramic composites as a function of microstructure: I. Numerical Simulation. J. Mech. Phys. Solids, http://dx.doi.org/10.1016/j.jmps.2012.09.013, in press.
Martin, E., Leguillon, D., Lacroix, C., 2001. A revisited criterion for crack deflection at an interface in a brittle bimaterial. Compos. Sci. Technol 61, 1671–1679.
Martínez, D., Gupta, V., 1994. Energy criterion for crack deflection at an interface between two orthotropic media. J. Mech. Physics. Solids 42, 1247–1271.
Miserez, A., Müller, R., Rossoll, A., Weber, L., Mortensen, A., 2004. Particle reinforced metals of high ceramic content. Mater. Sci. Eng., A 387–389, 822–831.
Parmigiani, J.P., Thouless, M.D., 2006. The roles of toughness and cohesive strength on crack deflection at interfaces. J. Mech. Physics. Solids 54, 266–287.
Rice, J.R., 1988. Elastic Fracture Mechanics Concepts for Interfacial Cracks. J. Appl. Mech. 55, 98–103.
Roger, R, N., 1998. The design of the fibre-matrix interfacial zone in ceramic matrix composites. Composites Part A 29, 1145–1155.
Veljkovic, J., 2005. The crack kinking out of an interface. Theoret. Appl. Mech 32, 209–221.
Warrier, S.G., Majumdar, B.S., Miracle, D.B., 1997. Interface effects on crack deflection and bridging during fatigue crack growth of titanium matrix composites. Acta Mater. 45, 4969–4980.
Zak, A.R., Williams, M.L., 1963. Crack Point Stress Singularities at a Bi-Material Interface. J. Appl. Mech. 30, 142–143.